

基础研究

慢性颈脊髓压迫症大鼠髓内基膜超微结构变化及其与 MMP-9 表达的相关性

徐晶辉¹, 龙厚清¹, 陈文立², 程 星¹, 于昊洋¹, 黄阳亮¹, 王晓波¹, 李佛保¹

(1 中山大学附属第一医院东院脊柱外科; 2 神经外科 510700 广州市)

【摘要】目的:观察慢性颈脊髓压迫症大鼠模型髓内基膜(basement membrane, BM)、基膜与星形细胞接触面(basement membrane-astrocyte contacts, BM-AC)的超微结构变化,并探讨其与基质金属蛋白酶-9(matrix metalloproteinase-9, MMP-9)表达的相关性。**方法:**72 只雄性 SD 大鼠随机分为对照组($n=36$)和实验组($n=36$),对照组仅切除 C5 左侧椎板;实验组在切除 C5 左侧椎板后将吸水可膨胀聚氨酯薄板置入 C6 水平左侧椎板下硬膜外,建立慢性颈脊髓压迫模型,应用 BBB(Basso Beattie Bresnahan)评分评价大鼠脊髓神经功能,并分别于造模后 1d、14d、21d、28d、42d、70d 取 C5~C6 段脊髓组织制备标本,用 HE 染色观察脊髓形态学变化、用 MMP-9 免疫组化染色检测脊髓 MMP-9 表达量,用透射电镜观察脊髓 BM 及 BM-AC 的变化。**结果:**对照组各时间点 BBB 评分和实验组造模后 1d 的 BBB 评分无显著性差异,实验组造模后 14d~70d 的 5 个时间点 BBB 评分均显著性低于同时点对照组($P<0.05$)。HE 染色显示对照组各时间点及实验组造模后 1d 的脊髓未见受压,脊髓形态结构正常;实验组造模后 1d 可见脊髓白质区轻度水肿;造模后 14d 脊髓受压变形,灰质区血管增生,灰质、白质水肿,神经元细胞核碎裂;造模后 21d 和 28d 损伤逐渐加重;造模后 42d 脊髓水肿减轻,髓内空泡化,前角大运动神经元数目减少、胞浆稀少、胞核萎缩,突触减少,神经纤维稀疏,髓鞘层变薄;造模后 70d 仍见白质区水肿、神经元细胞核碎裂,灶性胶质细胞增生等退行性变,神经元数目增多。MMP-9 免疫组化显示对照组各时间点及实验组造模后 1d、70d 脊髓 MMP-9 均呈弱表达,实验组造模后 14d 呈较强表达,21d 呈强表达,28d 呈较强表达,42d 呈中度表达。对照组各时间点及实验组压迫后 1d 的 BM 电子密度及 BM-AC 均正常,实验组造模后 14d~28d BM 电子密度、BM-AC 比率与对照组比较显著性降低($P<0.05$);实验组造模后 42d、70d 两者较前升高($P<0.05$),但仍显著低于对照组水平($P<0.05$)。MMP-9 表达与 BM 电子密度及 BM-AC 变化呈负相关,相关系数分别为 -0.892 ($P<0.001$)和 -0.664 ($P<0.001$)。**结论:**慢性颈脊髓压迫性损伤后早期髓内 BM 降解、BM-AC 分离,后期部分修复。MMP-9 可能通过降解 BM 及 BM-AC 影响脊髓压迫后血脊髓屏障的完整性。

【关键词】基膜;慢性脊髓压迫;超微结构;基质金属蛋白酶-9;大鼠

doi: 10.3969/j.issn.1004-406X.2016.02.11

中图分类号:R683.2, Q421 文献标识码:A 文章编号:1004-406X(2016)-02-0162-09

Ultrastructural changes of microvascular basement membrane and correlation with MMP-9 expression in rat model with chronic cervical cord compression/XU Jinghui, LONG Houqing, CHEN Wenli, et al//Chinese Journal of Spine and Spinal Cord, 2016, 26(2): 162-170

【Abstract】 Objectives: To investigate the temporal ultrastructural changes of microvascular basement membrane(BM) and basement membrane astrocyte contacts(BM-AC) in rat model with chronic cervical cord compression, and to explore their correlation with the expression of matrix metalloproteinase-9(MMP-9). **Methods:** 72 SD rats were randomly divided into the control group($n=36$) and the experimental group($n=36$). In the control group, C5 left semi-laminectomy was performed in each rat. In the experimental group, a water-absorbable polyurethane polymer was implanted into C6 left epidural space after C5 left semi-laminectomy. The Basso Beattie Bresnahan(BBB) score was used to evaluate the neurological function. HE staining, immunohistochemical staining and transmission electron microscopy(TEM) were performed at 1 day, 14 days, 21 days, 28 days, 42 days and 70 days after modeling to observe the changes of morphology, MMP-9 expression and ultrastructural changes of BM and BM-AC. **Results:** According to the BBB score, there was no significant dif-

基金项目:国家自然科学基金项目(编号:81450020);广东省自然科学基金项目(编号:S2013010015778)

第一作者简介:男(1989-),医师,硕士在读,研究方向:脊柱外科

电话:(020)82379597 E-mail:jinghui_xu1989@163.com

通讯作者:龙厚清 E-mail:hongqinglong@163.com

ference between each time point in the control group and one day after modeling in the experimental group, neurological function in the experimental group showed an obvious decline from 14 days to 70 days after modeling ($P < 0.05$). HE staining showed intact spinal cords at each time point in the control group. In the experimental group, a mild edema in white matter without spinal cord compression was shown at 1 day after modeling. The compressive deformation of spinal cord, vascular proliferation in grey matter, edema in white and grey matter and the fragmentation of nucleus in neurons were shown at 14 days after modeling. The damage was aggravated at 21 days and 28 days after modeling. At the 42th day after modeling, decreasing of edema in the spinal cord, intramedullary cavity, reducing number of motor neurons in the front foot of spinal cord, sparse cytoplasm, shrinking nucleus, reducing number of synapsis, sparse nerve fibers, the thinner layer of myelin were found. At the 70th day in the experimental group, edema in the white matter, the fragmentation of nucleus in neurons, focal hyperplasia of glial cells, increasing number of neurons were shown. The immunohistochemical staining displayed that MMP-9 was weakly expressed in the control group, and the same results were found at 1 day and 70 days after modeling in the experimental group. Strong expression of MMP-9 was found at 14 days and 28 days after modeling in the experimental group, strongest expression at 21 days after modeling, and moderate expression at 42 days after modeling in the experimental group. The proportion of BM-AC and electron density of BM in the experimental group decreased significantly at 14-28 days after modeling, and improved since the 42nd day after modeling (including the 70th day), but were still significantly lower than those in the control group ($P < 0.05$). There was no significant difference between each time point in the control group and 1 day after modeling in the experimental group. MMP-9 expression was negatively correlated with the proportion of BM-astrocyte contacts ($r = -0.664$, $P < 0.001$) and the BM density ($r = -0.892$, $P < 0.001$). **Conclusions:** The BM and BM-AC are damaged after chronic cervical cord compression and rehabilitated incompletely at late stage. MMP-9 may affect the integrity of blood-spinal cord barrier by degrading the BM and BM-AC after spinal cord compression.

【Key words】 Basement membrane; Chronic spinal cord compression; Ultrastructure; MMP-9; Rat

【Author's address】 Department of Spine Surgery, the Eastern Hospital of the First Affiliated Hospital of Sun Yat-sen University, Guangzhou, 510700, China

慢性颈脊髓压迫症是中老年人脊髓功能障碍最常见的病症之一^[1]。随着慢性脊髓压迫动物模型的建立和改进^[2,3],对其发病机制的认识也显著提高。研究表明血-脊髓屏障 (blood-spinal cord barrier, BSCB) 破坏是其病理生理改变的一个关键环节^[4]。有研究发现, BSCB 破坏与 MMP-9 高表达显著相关^[5,6]; Noble 等^[7]发现在 MMP-9 缺陷型大鼠脊髓损伤模型中 BSCB 损伤较野生型大鼠脊髓损伤模型显著减轻, 浸润的中性粒细胞表达 MMP-9 减低, 运动恢复较显著; 伤后 3h~3d 给予 MMP-9 拮抗剂可以得到与 MMP-9 缺陷型大鼠相似的结果, 提示 MMP-9 可能是引起 BSCB 破坏的重要因子, 但是 MMP-9 引起 BSCB 变化的具体机制不明。基膜 (BM) 电子密度和基膜与星形细胞接触面 (BM-AC) 比率是反应细胞外基质超微结构变化的重要指标^[8]。本研究应用已成功建立的慢性脊髓压迫大鼠模型^[9], 对造模后不同时间点脊髓组织中 MMP-9 表达、BM 及 BM-AC 超微结构变化特征进行动态观察, 并探讨二者的相关性。

1 材料与方法

1.1 动物模型的制备

3 月龄健康雄性 Sprague-Dawley (SD) 大鼠 72 只, 体重 340~360g (购自中山大学实验动物中心)。随机分为对照组和实验组, 每组 36 只。用 10% 水合氯醛腹腔注射麻醉 (3ml/kg) 后, 逐层切开显露 C5~C7 椎板, 切除 C5 椎板及椎板间黄韧带, 仔细分离下面的硬脊膜, 避免脊髓损伤、脑脊液渗漏。对照组仅切除椎板, 实验组使用手术显微镜将可吸水性聚氨酯聚合物薄板 (3×1×0.8mm) 嵌入 C6 椎板和硬脊膜之间, 聚合物薄板吸水后慢慢膨胀, 形成对脊髓慢性、渐进性、持续压迫^[2]。逐层缝合、关闭切口, 在加热床上恢复后, 分笼饲养, 大鼠在笼中可自由活动、获取食物和水。前期研究已经证实该模型的可靠性^[10]。

1.2 大鼠脊髓功能评价

采用 BBB 评分、双盲法对大鼠进行为期 70d 的行为学评分, 每只大鼠双后肢分别评分, 测试 3 次取平均值, 比较两组各时间点的 BBB 评分。

1.3 取材与标本制作

两组分别于造模后 1d、14d、21d、28d、42d、70d 分批取材, 每组每个时间点 6 只。用 10% 水合氯醛腹腔麻醉后 (5ml/kg), 快速取出颈段脊髓, 置于预冷蜡板, 快刀切取 C5~C6 脊髓 (5~8mm, 去掉脊膜), 迅速置入前固定液, 低温 (4℃) 固定 2~3d, 从中间横断成两半, 一半常规制备石蜡包块, 用于 HE 染色及免疫组化染色; 另一半选取 C6 颈髓左侧的灰质部分, 修成 1×1×1mm 的小块, 用 6.5% 蔗糖-磷酸缓冲液漂洗, 2% 锇酸缓冲液固定 1h, 乙醇逐级脱水, Epon812 环氧树脂包埋, 置自动烤箱加温聚合, 解剖镜下修整组织块, 暴露出脊髓横断面, 于低倍显微镜下切取脊髓, 修整后行 70nm 超薄切片, 铀-铅双重染色后用于透射电镜 (TME, Philips CM 10, Eindhoven, Holland) 观察。

1.4 组织学检测

石蜡包块连续切成厚 5 μ m 切片, 取相邻切片分别进行 HE 染色及免疫组化染色。HE 染色观察脊髓的形态变化; 免疫组化染色后采用 S-P 法半定量检测 MMP-9 表达量, 观察表达部位, 使用 MMP-9 羊抗鼠单克隆抗体即用型 (Abcam plc) 及 S-P 免疫组化试剂盒 (上海基因生物技术公司), 严格按试剂盒推荐方法操作, 以 PBS 代替一抗为阴性对照。免疫组化图片均在同一条件下拍摄, 拍摄过程除焦距外其他参数均保持一致。对图片随机编号。用 Image Pro Plus (version 6.0, Media Cybernetics, Inc., Bethesda, MD, USA) 测量 MMP-9 免疫组化染色强度。MMP-9 免疫组化强度用 OD (optical density) 来表示, OD=免疫染色的

累积光密度 (IOD)/面积 (Area)。测量前对图片中最亮空白处进行光密度统一校正。免疫组化染色范围统一在 HIS 选色 (H:0-29, S:0-255, I:0-210)。

1.5 电镜检测

所有电镜图片均在同一条件下拍摄, 拍摄过程除焦距外其他参数均保持一致。对图片随机编号。用 Image Pro Plus 测量 BM-AC 比率 (BM-AC ratio, BM-ACR) 和 BM 平均电子密度。BM-ACR=基膜-星形胶质细胞接触长度/微血管周长 (基底膜长度)×100% (图 1), BM 平均电子密度 OD=IOD/Area。

1.6 统计学分析

应用 SPSS 16.0 软件 (SPSS 公司, 美国) 进行统计分析。计量资料以 $\bar{x}\pm s$ 表示。两组相同时间点 BBB 评分比较采用两独立样本 *t* 检验, 同一组不同时间点比较采用重复测量数据的方差分析, 进一步的两两比较采用 LSD-*t* 检验; 两组间 BM 平均电子密度 OD 值、BM-ACR 与免疫组化 MMP-9 OD 值的比较采用两样本的秩和检验, 组内各时间点的比较采用 Kruskal-Wallis 秩和检验; BM 平均电子密度 OD 值、BM-ACR 与免疫组化 MMP-9 OD 值的相关性运用 Spearman 检验。检验水准 α 值取双侧 0.05。

2 结果

大鼠均造模成功, 在取材前均未出现死亡。

2.1 BBB 评分

造模后各时间点两组大鼠 BBB 评分见表 1。

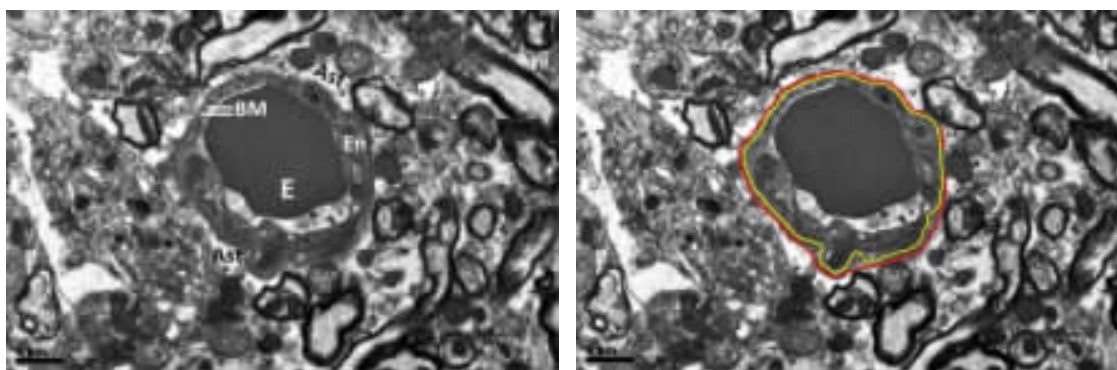


图 1 电镜下脊髓微血管各结构 a 星形胶质细胞足突 (Ast)、基膜 (BM)、内皮细胞 (En)、红细胞 (E) ($\times 9\ 700$) b 基膜与星形胶质细胞足突接触比率=基膜与星形胶质细胞接触长度 (红线)/包绕微血管基膜的长度 (黄线)×100%

Figure 1 The diagram of the ultrastructure of the microvascular in spinal cord a Ast, astrocyte endfeet; BM, basement membrane; En, endothelial cell; E, erythrocyte (Original magnification $\times 9\ 700$) b Measurement of the basement membrane and astrocyte endfeet contact. The proportion of the intact contact is calculated as [length of intact BM-astrocyte contact (red lines)/total circumferential length of the microvascular BM (yellow line) $\times 100\%$]

对照组各时间点间 BBB 评分无显著性差异 ($P>0.05$); 实验组造模后 1d 与对照组比较无显著性差异 ($P>0.05$), 造模后 14d 时 BBB 评分下降, 21d 达到最低, 42d 后 BBB 评分升高, 到 49d 后基本保持稳定, 14d、21d、28d、42d、70d 时的 BBB 评分与同时点对照组比较显著性降低 ($P<0.05$)。

2.2 组织学特征

对照组各时间点 HE 染色显示大鼠正常脊髓的组织学结构特征。实验组造模后 1d 可见脊髓形态正常; 造模后 14d 可见脊髓受压变形, 灰质区血管增生, 灰质、白质水肿, 可见神经元细胞核碎裂; 造模后 21d 脊髓水肿明显, 中央管扩大变形、静脉淤血, 神经元数目减少、梭形变, 白质后索神经纤维排列紊乱、部分轴索细网断裂; 造模后 28d 脊髓白质区水肿、灰质血管增生及坏死、神经元细胞核碎裂均较 21d 加重; 造模后 42d 脊髓水肿减轻, 髓内空泡化, 前角大运动神经元数目减少、胞浆稀少、胞核萎缩, 突触减少, 神经纤维稀疏, 髓鞘层变薄; 造模后 70d 仍见白质区水肿、神经元细胞核碎裂, 灶性胶质细胞增生等退行性变, 神经元数目增多(图 2)。

2.3 MMP-9 免疫组化表达

对照组各时间点脊髓内 MMP-9 均仅有微弱表达, 各时间点无显著性差异。造模后 1d, MMP-9 微弱表达, 与对照组比较无显著性差异; 造模后 14d, MMP-9 在细胞胞质中及细胞外基质中均有较强表达; 造模后 21d, 胞质及细胞外基质均强表达, 分布均匀, 表达强度最高; 造模后 28d, 胞质及细胞外均有较强表达, 以细胞外基质为主; 造模后 42d, 细胞外基质中度表达, 胞质中微弱表达; 造模后 70d, 细胞外基质有微弱表达, 与对照组及实验组造模后 1d 时表达程度相似。实验组造模后 14d~70d 的 MMP-9 表达随时间由胞质内逐渐到细胞外基质, 表达由弱到强再到弱(图 3、表 2)。

2.4 BM 超微结构变化

对照组各时间点微血管中 BM 黑色均匀, 轮廓完整清晰, 单层包绕在血管内皮细胞外面, 各时间点均显示正常微血管超微结构, BM OD 值无显著性差异。实验组造模后 1d, 微血管超微结构、BM OD 值与对照组无明显差异; 造模后 14d, 实验组微血管中 BM 电子密度轻度降低, 轮廓模糊但仍可辨认, 星形胶质细胞水肿, 可见 BM 与星形胶质细胞足突分离; 造模后 21d, 微血管 BM 电子密度显著降低, 与星形胶质细胞足突明显分离, 星

表 1 对照组与压迫组各时间点 BBB 评分 ($\bar{x}\pm s$)

Table 1 Average BBB score of the two groups

造模后时间 Time	n	对照组 Control group	实验组 Experimental group
1d	36	19.70±0.67	19.71±0.64
14d	30	19.80±0.78	17.57±0.87 ^①
21d	24	19.90±0.87	15.95±0.67 ^①
28d	18	19.90±0.67	15.43±0.59 ^①
42d	12	20.00±0.81	16.10±0.83 ^{①②}
70d	6	19.90±0.88	16.80±0.67 ^{①②}

注: ①与同时点对照组比较 $P<0.05$; ②与同组 28d 时比较 $P<0.05$

Note: ①Compared with control group at the same time, $P<0.05$; ②compared with the 28th day of the same group, $P<0.05$

形胶质细胞水肿, 部分坏死; 造模后 28d, 微血管 BM 电子密度明显降低, 轮廓模糊不清, 与星形胶质细胞足突大部分分离, 周围坏死加重。造模后 42d, 微血管电子 BM 密度明显升高, 与星形胶质细胞足突间的接触面绝大部分贴合, 周围坏死减轻; 造模后 70d, 实验组 BM 电子密度基本接近正常, 轮廓清晰, 出现双层 BM, 与星形胶质细胞突触接触面基本贴合, 出现代偿性增生改变(图 4)。实验组中微血管 BM 电子密度定量 OD 值改变先降低后升高, 在 21d 时 OD 值最低, 28d 次之, 到 42d、70d 基本稳定(表 2)。

2.5 BM-ACR 变化

对照组各时间点的 BM-ACR 无显著性差异。实验组造模后 1d 时 BM-ACR 与对照组比较无显著性差异 ($P>0.05$), 造模后 14d 时 BM-ACR 有所下降; 21d 时降至最低; 28d 时较第 21 天略有升高; 42d 时明显升高; 70d 时较 42d 时升高的幅度不大, 与对照组比较还有一定差距。在 14d、21d、28d、42d、70d 时与对照组比较均有显著性差异(表 2, $P<0.05$)。

2.6 MMP-9 表达与 BM 密度、BM-ACR 之间的相关性

BM-ACR 与 BM 平均电子密度呈正相关 ($r=0.731, P<0.001$); MMP-9 表达强度与 BM 平均电子密度呈负相关 ($r=-0.892, P<0.001$); MMP-9 表达强度与 BM-ACR 呈负相关 ($r=-0.664, P<0.001$)。三者随时间的变化趋势见图 5。

3 讨论

成功构建动物模型是研究慢性颈脊髓压迫症发病机制的重要前提。对致压材料的膨胀速率、体积、脊髓压迫比等的系列研究^[2,9,10], 验证了本研究

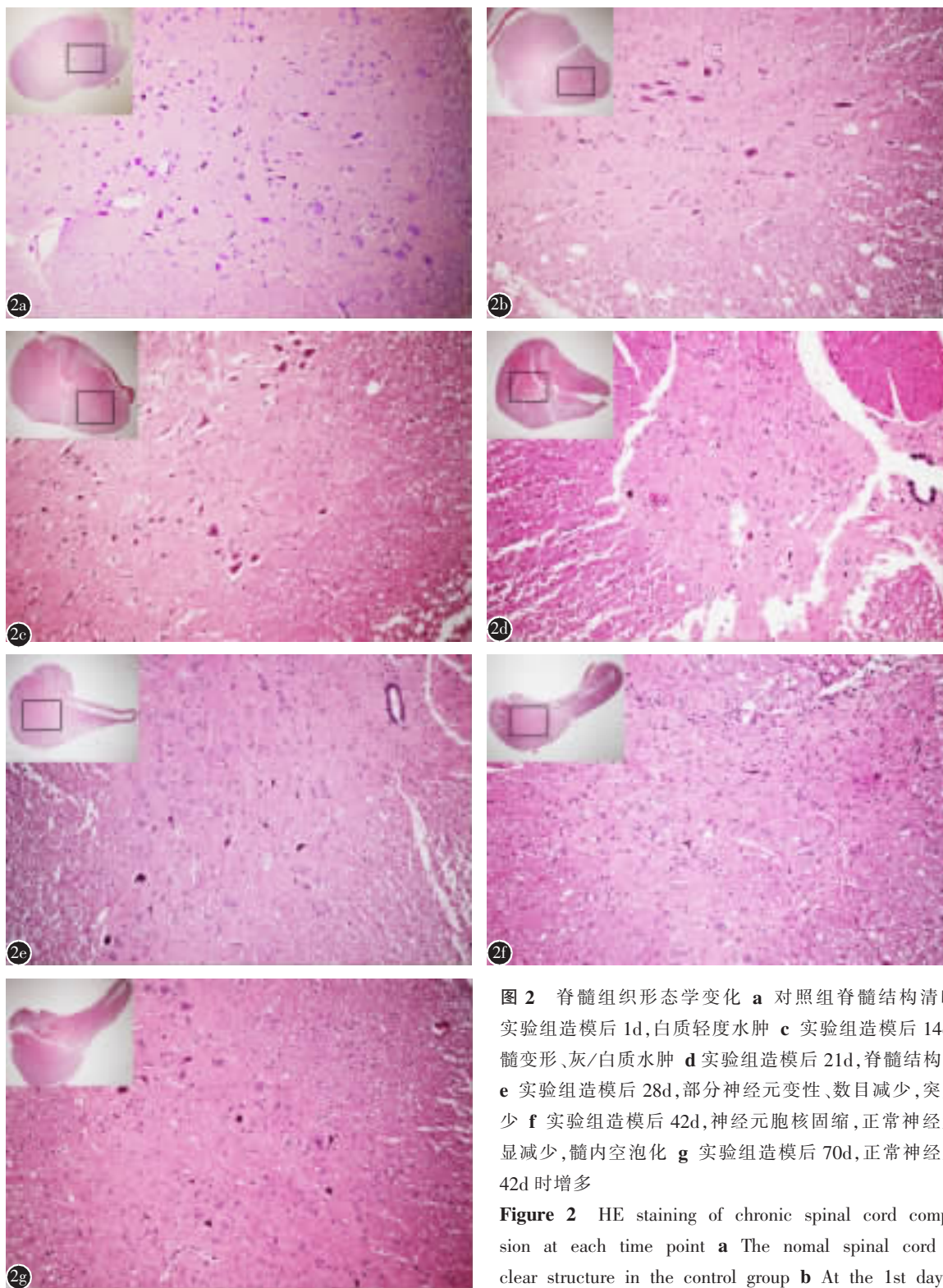


图 2 脊髓组织形态学变化 **a** 对照组脊髓结构清晰 **b** 实验组造模后 1d, 白质轻度水肿 **c** 实验组造模后 14d, 脊髓变形、灰/白质水肿 **d** 实验组造模后 21d, 脊髓结构紊乱 **e** 实验组造模后 28d, 部分神经元变性、数目减少, 突触减少 **f** 实验组造模后 42d, 神经元胞核固缩, 正常神经元明显减少, 髓内空泡化 **g** 实验组造模后 70d, 正常神经元较 42d 时增多

Figure 2 HE staining of chronic spinal cord compression at each time point **a** The normal spinal cord with clear structure in the control group **b** At the 1st day after modeling in the experimental group, mild edema was observed in white matter **c** At the 14th day after modeling in the experimental group, compression and edema of spinal cord were observed **d** At the 21st day after modeling in the experimental group, disorder of structure were observed in the spinal cord **e** At the 28th day after modeling in the experimental group, degeneration of some neuron and decrease in the number of synapse and neuron were observed **f** At the 42nd day after modeling in the experimental group, pycnosis of nucleus in neurons, intramedullary vacuolation in spinal cord, and decrease in the number of normal neuron were observed **g** At the 70th day after modeling in the experimental group, more normal neurons were observed than the 42nd day after modeling

ter modeling in the experimental group, mild edema was observed in white matter **c** At the 14th day after modeling in the experimental group, compression and edema of spinal cord were observed **d** At the 21st day after modeling in the experimental group, disorder of structure were observed in the spinal cord **e** At the 28th day after modeling in the experimental group, degeneration of some neuron and decrease in the number of synapse and neuron were observed **f** At the 42nd day after modeling in the experimental group, pycnosis of nucleus in neurons, intramedullary vacuolation in spinal cord, and decrease in the number of normal neuron were observed **g** At the 70th day after modeling in the experimental group, more normal neurons were observed than the 42nd day after modeling

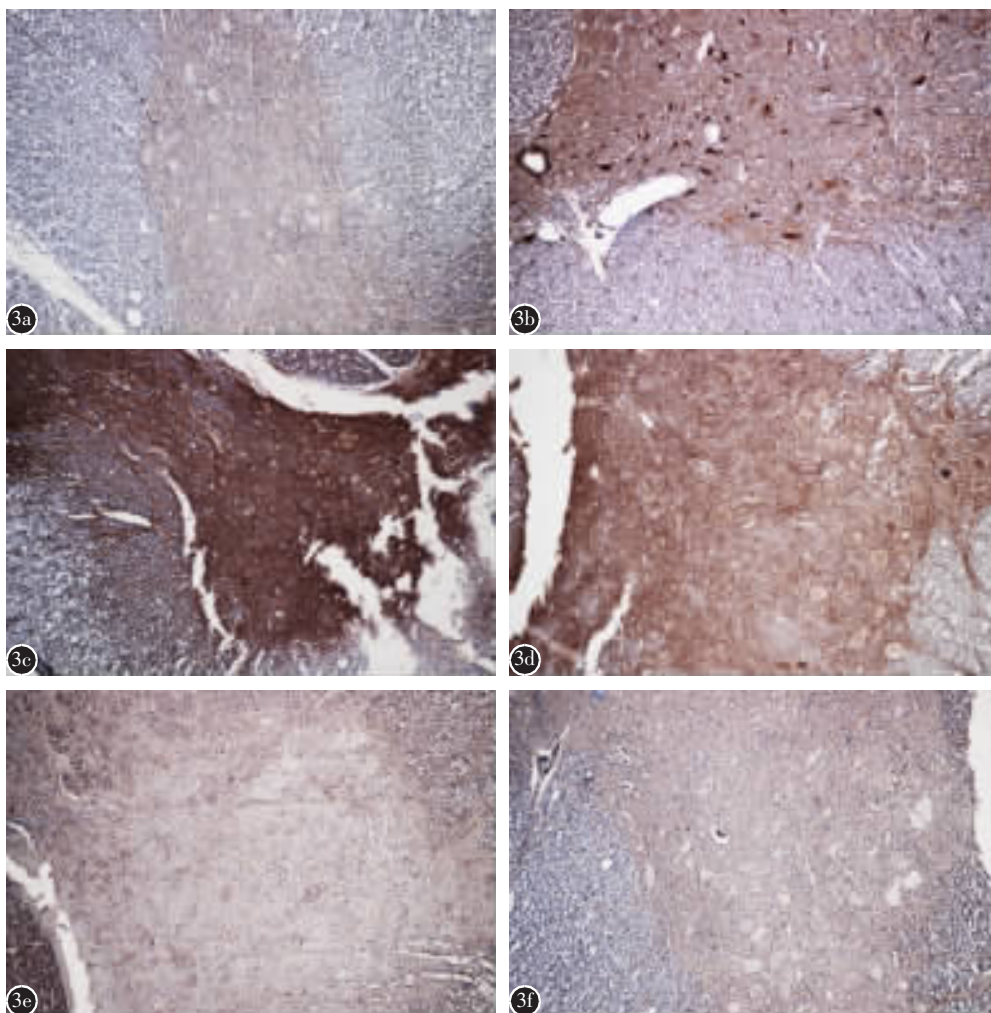


图 3 MMP-9 免疫组化染色 a 对照组脊髓中胞质中微弱表达 b 实验组造模后 14d,胞质强中表达,细胞外基质中度表达 c 实验组造模后 21d,胞质及细胞外基质中 MMP-9 均强表达,分布较均匀 d 实验组造模后 28d,胞质及细胞外基质中 MMP-9 均较强表达,以细胞外基质为主 e 实验组造模后 42d,细胞外基质中 MMP-9 中度表达,细胞质中微弱表达 f 实验组造模后 70d,仅细胞质中微弱表达($\times 200$)

Figure 3 Immunohistochemical staining of MMP-9 a In the control group, weak cytoplasmic expression of MMP-9 was observed in the spinal cord b At the 14th day after modeling in the experimental group, high cytoplasmic expression of MMP-9 was observed in the spinal cord. Note that the moderate expression of MMP-9 was observed in the extracellular matrix c At the 21st day after modeling in the experimental group, strong expression of MMP-9 was observed both in the cytoplasm and the extracellular matrix d At the 28th day after modeling in the experimental group, strong expression of MMP-9 was observed both in the cytoplasm and the extracellular matrix, predominantly in the extracellular matrix e At the 42nd day after modeling of the experimental group, moderate expression of MMP-9 was observed in the spinal cord, mainly in the extracellular matrix f At the 70th day after modeling in the experimental group, weak cytoplasmic expression of MMP-9 was observed in the spinal cord(magnification $\times 200$)

应用的慢性颈脊髓压迫症模型的病理学、影像学 and 神经行为学特征与临床 CSM 符合度较高。目前,有多家研究机构采用或参考该模型开展相关研究^[3,11,12]。

我们应用该模型研究发现,慢性压迫性脊髓损伤伴随着不同程度的 BSCB 破坏,但其确切机制不明^[4,5]。BSCB 是隔离脊髓实质微环境与血循

环的屏障结构,由无孔内皮细胞、BM、星形胶质细胞足突及周细胞组成^[13],BM 内侧粘附无孔内皮细胞,外侧被星形胶质细胞足突通过各种粘附分子包绕,是 BSCB 中支持、连接各细胞成分的重要框架,也是血循环与胶质细胞、周细胞、神经元等进行信号传导和物质转运的基本屏障^[14]。因此,BM 的完整性对于维持 BSCB 正常功能至关重要。BM

表 2 对照组与实验组不同时间点 BM OD 值、BM-ACR 及 MMP-9 OD 值 ($\bar{x}\pm s, n=6$)

Table 2 BM OD, BM-ACR and MMP-9 OD in the two groups at each time point

	BM OD		BM-ACR		MMP-9	
	对照组 Control group	实验组 Experimental group	对照组 Control group	实验组 Experimental group	对照组 Control group	实验组 Experimental group
1d	0.625±0.015	0.625±0.015	0.955±0.024	0.958±0.020	0.016±0.005	0.016±0.003
14d	0.630±0.014	0.456±0.013 ^①	0.939±0.052	0.814±0.076 ^①	0.017±0.003	0.114±0.007 ^①
21d	0.638±0.021	0.378±0.009 ^①	0.915±0.045	0.392±0.099 ^①	0.018±0.004	0.157±0.006 ^①
28d	0.641±0.029	0.484±0.013 ^①	0.960±0.038	0.411±0.096 ^①	0.017±0.004	0.131±0.013 ^①
42d	0.622±0.020	0.581±0.010 ^{①②}	0.963±0.024	0.705±0.084 ^{①②}	0.016±0.004	0.040±0.012 ^{①②}
70d	0.622±0.014	0.586±0.015 ^{①②}	0.940±0.018	0.717±0.067 ^{①②}	0.015±0.003	0.014±0.003 ^②

注:①与同时间点对对照组比较 $P<0.05$; 与同组 28d 时比较 $P<0.05$

①Compared with control group at the same time, $P<0.05$; ②Compared with the 28th day of the same group, $P<0.05$

主要由 IV 型胶原、层粘连蛋白、纤连蛋白、硫酸乙酰肝素、蛋白聚糖等构成^[15], 可被细胞外基质降解酶如 MMPs 降解, MMP 降解 ECM、改变细胞外微环境、促进细胞迁徙和 ECM 重构^[16]。本研究发现, 在脊髓受压后早期 BM 出现不同程度的电子密度降低, 提示 BM 降解, 但在受压后期 BM 呈现一定程度的修复现象, 同时脊髓功能亦得到一定程度的改善, 而同期的 MMP-9 的表达趋势与之相反。我们的前期研究也发现, BSCB 破坏与 MMP-9 高表达显著相关^[5], 而 MMP-9 可作用于 BSCB 基本结构 BM 的主要成分: IV 型胶原、层粘连蛋白和纤粘连蛋白等^[17]。因此我们认为, 脊髓受压后 MMP-9 表达增高、进而降解 BM, 可能是脊髓慢性压迫性损伤后 BSCB 破坏的重要机制之一。

有研究发现, 在大鼠急性脊髓损伤后, 阻断 MMP-9 活性, 其神经功能得到明显改善^[18]; 在脑缺血大鼠模型中, 黄体酮和四氢孕酮通过降低 MMP-9 表达, 减少紧密连接蛋白的降解^[19]; 在非人类灵长类、大鼠中有关脑卒中动物实验研究发现, 在阻断大脑中动脉 3h 再灌注 24h 后与对照组相比, IV 型胶原、层粘连蛋白、纤连蛋白丢失约 55%~70%^[20, 21]; 一项脊髓慢性压迫动物模型研究发现, 与对照组相比脊髓慢性压迫动物模型 BM 层粘连蛋白明显减少^[9]; 另一研究表明, 在大鼠脑卒中后 20h, BM 电子密度下降 71%^[8]。本研究结果发现实验组造模后 21d、28d, BM 电子密度下降了 36%~40%, 下降程度的差异性可能和急性缺血缺氧与慢性缺血缺氧的病理生理变化差异有关。

关于 BSCB 损伤修复的时间窗各研究的结果相差较大, 在以辣根过氧化酶为标记的大鼠模型中, BSCB 在伤后 14d 时得以重建^[22]; 另一项应用 AIB 为示踪剂的研究发现, 脊髓损伤后 14~28d 时

BSCB 通透性再次升高; 而应用动态强化对照磁共振 (dynamic contrast-enhanced magnetic resonance imaging, DCE-MRI) 研究发现, BSCB 损害一直持续到脊髓损伤后 56d^[23]。这些研究均提示 BSCB 在脊髓损伤过程中的变化是引起脊髓功能障碍的重要机制之一, 与我们前期的系列研究结果一致^[24, 25]。本研究中实验组造模后 42d 时 BM 开始修复重建, BM-ACR 和 BM 电子密度都有明显恢复, 脊髓神经功能也有一定程度恢复; 但即使到造模后 70d, BM-ACR 和 BM 电子密度均未能达到正常水平。这可能与星形胶质细胞瘢痕及新修复的 BM 各成分还不够成熟有关。

本研究结果显示, 慢性颈脊髓压迫症大鼠脊髓组织中 MMP-9 的表达特点为先增多后减少, 表达部位从以胞质为主到以细胞外基质为主, 随后回到胞质。这可能是脊髓受压后 MMP-9 在胞质内合成增多, 之后释放到细胞外基质。这种表达现象提示慢性压迫性脊髓损伤引起 MMP-9 的表达可能是一过性的, 而不是持续高表达。在新西兰兔慢性脊髓压迫模型中, 压迫 20 周后仍发现 MMP-9 的高表达^[9]。本研究为大鼠慢性脊髓压迫模型, 到造模后 42d 时表达已经降低, 这可能是不同模型动物表达时间窗差异。一项脑卒中研究发现, 基膜-星形胶质细胞足突分离先于 MMP-9 高表达和 BM 电子密度减低^[8], 提示除 MMP-9 外可能还有其他细胞外基质降解酶在起作用。引起 MMP-9 高表达的因素可能包括机械压迫引起的缺血缺氧^[26]、触发 NF- κ B 通路^[27]等, 但其确切机制有待进一步研究。

总之, 慢性压迫性颈脊髓损伤后早期 (14d~28d) 髓内 BM 降解、BM-AC 分离, 后期 (42d~70d) BM 部分修复。MMP-9 表达与之呈负相关, MMP-

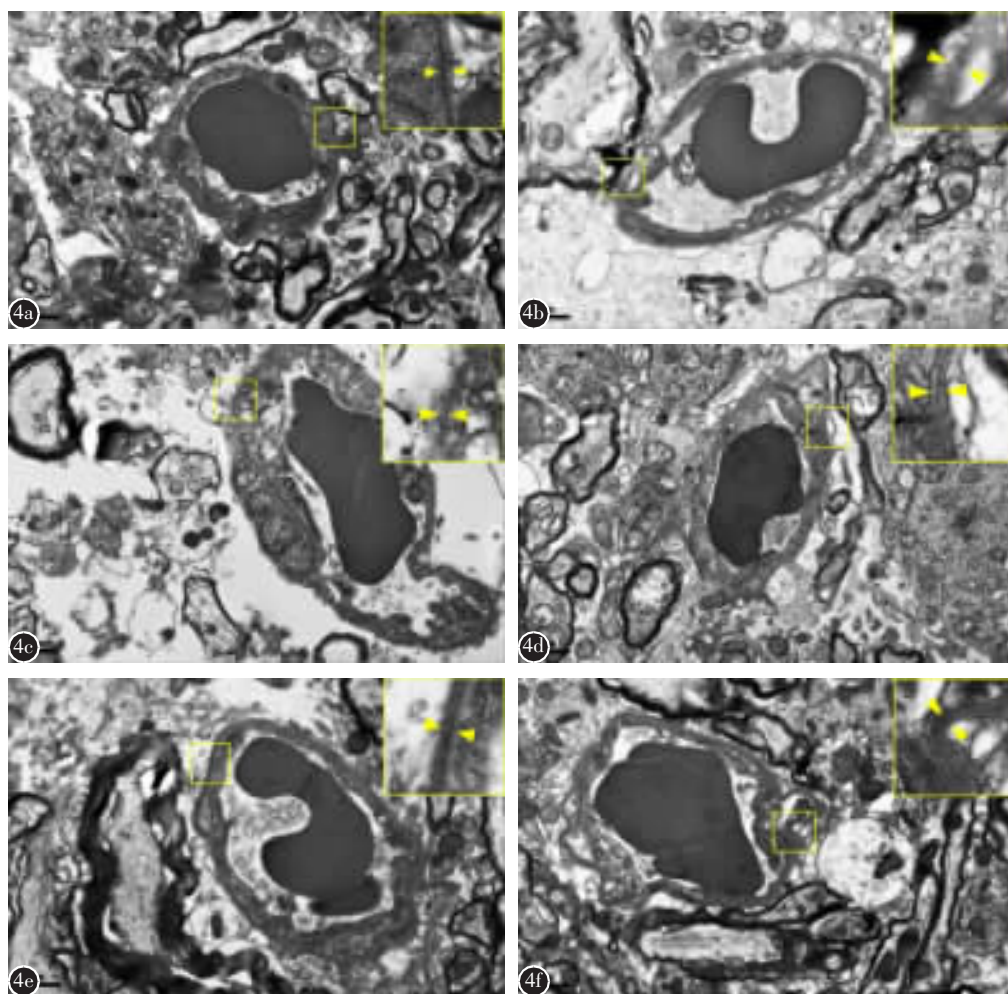


图 4 电镜观察 a 对照组正常 BM、星形胶质细胞足突 b 实验组造模后 14d 时 BM 密度降低,与星形胶质细胞足突分离 c 实验组造模后 21d 时 BM 密度明显降低,与星形胶质细胞足突基膜多处分离,细胞明显水肿 d 实验组造模后 28d 时,微血管周围水肿,BM 密度明显降低,星形胶质细胞破裂 e 实验组造模后 42d 时,基膜密度明显增高,与星形胶质细胞接触面明显升高 f 实验组造模后 70d 时,微血管完整,可见双层 BM,与星形胶质细胞接触面明显增加 (×9700) 图 5 实验组 BM-ACR、BM 平均电子密度和 MMP-9 表达水平随时间变化趋势图

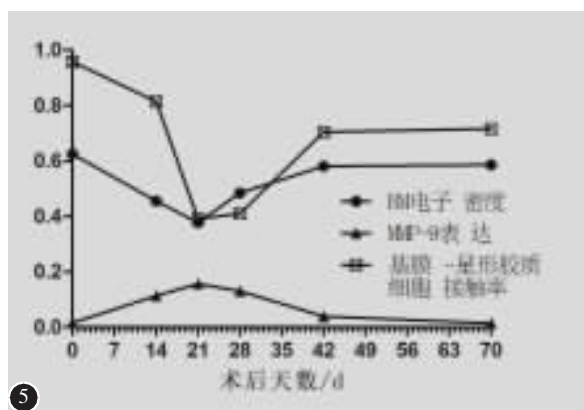


Figure 4 Representative electron microscopic photographs a In the control group, normal BM, almost all surface areas of the microvessel are covered by astrocyte endfeet b At the 14th day after modeling in the experimental group, decreasing of BM electron density and focal detachment of the astrocyte endfeet from the basement membrane (BM) were observed c At the 21st day after modeling in the experimental group, a significant decreasing of BM electron density, a marked astrocyte swelling and a further decrease in the intact portion of the contacts were demonstrated d At the 28th day after modeling in the experimental group, excessive accumulation of water around the microvessels, further degradation of the BM and ruptured astrocytes were observed e At the 42nd day after modeling in the experimental group, the electron density of BM and the proportion of the intact BM-astrocyte contacts was markedly increased f At the 70th day after modeling, capillary integrity, double layers of endothelial cells and basement membranes could be seen. Arrowheads in the inset (magnified view) indicate the BM. Original magnification is 9 700 Figure 5 The temporal pattern of the BM-astrocyte contacts, BM electron density, and MMP-9 expression

9可能通过降解 BM 及 BM-AC 影响脊髓压迫后血-脊髓屏障的完整性。

4 参考文献

- Kalsi-Ryan S, Karadimas SK, Fehlings MG. Cervical spondylotic myelopathy: the clinical phenomenon and the current pathobiology of an increasingly prevalent and devastating disorder[J]. *Neuroscientist*, 2013, 19(4): 409-421.
- 龙厚清, 温春毅, 胡勇, 等. 慢性压迫性脊髓症研究平台的建立及体感诱发电位功能评价的机制[J]. *中华骨科杂志*, 2010, 30(4): 427-432.
- Karadimas SK, Moon ES, Yu WR, et al. A novel experimental model of cervical spondylotic myelopathy(CSM) to facilitate translational research[J]. *Neurobiol Dis*, 2013, 54: 43-58.
- Karadimas SK, Gatzounis G, Fehlings MG. Pathobiology of cervical spondylotic myelopathy [J]. *Eur Spine J*, 2015, 24 (Suppl 2): 132-138.
- 龙厚清, 陈文立, 谢文林, 等. 慢性压迫性脊髓症基质金属蛋白酶-9 表达与血脊髓屏障破坏的相关性研究[J]. *中华骨科杂志*, 2015, 35(4): 456-462.
- Karadimas SK, Klironomos G, Papachristou DJ, et al. Immunohistochemical profile of NF- κ B/p50, NF- κ B/p65, MMP-9, MMP-2, and u-PA in experimental cervical spondylotic myelopathy[J]. *Spine*, 2013, 38(1): 4-10.
- Noble LJ, Donovan F, Igarashi T, et al. Matrix metalloproteinases limit functional recovery after spinal cord injury by modulation of early vascular events[J]. *J Neurosci*, 2002, 22 (17): 7526-7535.
- Kwon I, Kim EH, del Zoppo GJ, et al. Ultrastructural and temporal changes of the microvascular basement membrane and astrocyte interface following focal cerebral ischemia[J]. *J Neurosci Res*, 2009, 87(3): 668-676.
- 李广盛, 龙厚清, 林尔坚, 等. 一种新型慢性压迫性颈髓损伤大鼠模型的建立[J]. *中华显微外科杂志*, 2013, 36(1): 46-51.
- Long HQ, Li GS, Lin EJ, et al. Is the speed of chronic compression an important factor for chronic spinal cord injury rat model[J]. *Neurosci Lett*, 2013, 545: 75-80.
- Zhang Z, Zhang YP, Shields LBE, et al. Technical comments on rodent spinal cord injuries models: neural regeneration research[J]. 2014, 9(5): 453-455.
- 王军, 容威, 刘忠军, 等. 大鼠慢性颈脊髓压迫减压术后神经功能改变及其相关机制探讨[J]. *中国脊柱脊髓杂志*, 2012, 22(8): 729-736.
- Bartanusz V, Jezova D, Alajajian B, et al. The blood-spinal cord barrier: morphology and clinical implications [J]. *Ann Neurol*, 2011, 70(2): 194-206.
- Kefalides NA, Alper R, Clark CC. Biochemistry and metabolism of basement membranes[J]. *Int Rev Cytol*, 1979, 61(1): 167-228.
- Martin GR, Timpl R. Laminin and other basement membrane components[J]. *Annu Rev Cell Bio*, 1987, 3(1): 57-85.
- Page-McCaw A, Ewald AJ, Werb Z. Matrix metalloproteinases and the regulation of tissue remodelling[J]. *Nat Rev Mol Cell Biol*, 2007, 8(3): 221-233.
- Vandooren J, Van den Steen PE, Opendakker G. Biochemistry and molecular biology of gelatinase B or matrix metalloproteinase-9 (MMP-9): the next decade [J]. *Crit Rev Biochem Mol Biol*, 2013, 48(3): 222-272.
- Noble LJ, Donovan F, Igarashi T, et al. Matrix metalloproteinases limit functional recovery after spinal cord injury by modulation of early vascular events[J]. *J Neurosci*, 2002, 22 (17): 7526-7535.
- Ishrat T, Sayeed I, Atif F, et al. Progesterone and allopregnanolone attenuate blood-brain barrier dysfunction following permanent focal ischemia by regulating the expression of matrix metalloproteinases[J]. *Exp Neurol*, 2010, 226(1): 183-190.
- Hamann GF, Okada Y, Fitridge R, et al. Microvascular basal lamina antigens disappear during cerebral ischemia and reperfusion[J]. *Stroke*, 1995, 26(11): 2120-2126.
- Vosko MR, Busch E, Burggraf D, et al. Microvascular basal lamina damage in thromboembolic stroke in a rat model [J]. *Neurosci Lett*, 2003, 353(3): 217-220.
- Maikos JT, Shreiber DI. Immediate damage to the blood-spinal cord barrier due to mechanical trauma [J]. *J Neurotrauma*, 2007, 24(3): 492-507.
- Cohen DM, Patel CB, Ahobila-Vajjula P, et al. Blood-spinal cord barrier permeability in experimental spinal cord injury: dynamic contrast-enhanced MRI[J]. *NMR Biomed*, 2009, 22 (3): 332-341.
- Long HQ, Xie WH, Chen WL, et al. Value of micro-CT for monitoring spinal microvascular changes after chronic spinal cord compression[J]. *Int J Mol Sci*, 2014, 15(7): 12061-12073.
- Cheng X, Long H, Chen W, et al. Three-dimensional alteration of cervical anterior spinal artery and anterior radicular artery in rat model of chronic spinal cord compression by micro-CT[J]. *Neurosci Lett*, 2015, 606: 106-112.
- Gaffney J, Solomonov I, Zehorai E, et al. Multilevel regulation of matrix metalloproteinases in tissue homeostasis indicates their molecular specificity in vivo [J]. *Matrix Biol*, 2015, 44-46: 191-199.
- Yeh CH, Lin YM, Wu YC, et al. Inhibition of NF- κ B activation can attenuate ischemia/reperfusion-induced contractility impairment via decreasing cardiomyocyte proinflammatory gene up-regulation and matrix metalloproteinase expression[J]. *J Cardiovasc Pharmacol*, 2005, 45(4): 301-309.

(收稿日期:2015-12-06 末次修回日期:2016-01-12)

(英文编审 唐翔宇/贾丹彤)

(本文编辑 卢庆霞)